BIOCELL

Tech Science Press

http://doi.org/10.32604/biocell.2026.085300

ARTICLE

Sevoflurane-Induced Pulmonary Microvascular Hyperpermeability via Upregulating EGR2

Zhuyuan Ren, Yong Chen, Jiaqiao Wu, Qiang Li and Qiang Fu*

Department of Anesthesiology, the Third People's Hospital of Chengdu, Chengdu, China
*Corresponding Author: Qiang Fu. Email: fuqiang1878@outlook.com

Received: 08 May 2026; Accepted: 23 June 2026; Published: 22 September 2026

ABSTRACT: Background: Volatile anesthetics such as sevoflurane are ubiquitous in perioperative care, yet their unintended consequences on pulmonary microvascular integrity and the upstream intracellular signaling pathways remain incompletely defined. This study elucidates the precise transcriptional mechanisms linking sevoflurane exposure to pulmonary endothelial hyperpermeability. **Methods:** Transendothelial electrical resistance (TEER) and macromolecular permeability were dynamically quantified in human pulmonary microvascular endothelial cell (HPMEC) monolayers following sevoflurane exposure. Global transcriptomic profiling (RNA-seq) was employed to identify core regulatory nodes, which were functionally validated via targeted siRNA silencing *in vitro* and subsequently corroborated in a murine model of clinical sevoflurane inhalation. **Results:** Sevoflurane (0.2–0.3 mM) induced a dose- and time-dependent disruption of endothelial barrier function, evidenced by a up to 2.5-fold increase in macromolecular permeability ($p < 0.001$) and a 64% reduction in transendothelial electrical resistance (TEER, dropping from ~28 to ~10 $\Omega \cdot cm^2$; $p < 0.001$). Unbiased transcriptomic analysis identified Early Growth Response 2 (EGR2) as the principal transcriptional driver. Sevoflurane provoked a 1.9-fold increase in EGR2 mRNA transcription ($p < 0.01$) and a >10-fold surge in its nuclear accumulation ($p < 0.01$), triggering profound downstream secretion of Vascular Endothelial Growth Factor (VEGF). Crucially, targeted knockdown of EGR2 abolished the sevoflurane-induced VEGF surge and fully preserved barrier integrity, restoring TEER and permeability to baseline control levels ($p < 0.001$ vs. sevoflurane alone). *In vivo* assessments confirmed that 3.3% sevoflurane inhalation significantly upregulates the pulmonary EGR2/VEGF axis, resulting in overt microvascular leakage and interstitial edema. **Conclusion:** Sevoflurane compromises pulmonary microvascular endothelium via the aberrant activation of the EGR2/VEGF signaling axis. Inhibiting EGR2 represents a novel, targeted therapeutic strategy to preserve vascular integrity and mitigate anesthetic-induced lung injury in susceptible surgical populations.

KEYWORDS: Sevoflurane; pulmonary microvascular endothelium; vascular permeability; early growth response 2 (EGR2); vascular endothelial growth factor (VEGF); perioperative lung injury

1 Introduction

The vascular endothelium constitutes a dynamic, highly selective semipermeable barrier that maintains tissue homeostasis, regulates the transvascular exchange of fluids and macromolecules, and coordinates local inflammatory responses [1–3]. Recent studies emphasize that endothelial barrier dysfunction, often exacerbated by oxidative stress and local inflammatory cascades, is a pivotal pathological event driving severe pulmonary vascular diseases [4]. Under physiological conditions, the structural integrity of this endothelial monolayer is tightly maintained by a complex, interdependent network of adherens junctions, tight junctions, and the underlying actin cytoskeleton. The dynamic regulation of these cytoskeletal

structures is driven by cellular biomechanical features, which play critical roles in evaluating and modulating endothelial cell behavior [5]. Disruption of this architecture results in increased microvascular permeability, a fundamental pathological process underlying pulmonary edema and acute lung injury [6–9]. Furthermore, the vascular microenvironment is tightly regulated by upstream stress-responsive transcriptional factors, which dynamically modify endothelial cell behavior and structural integrity under hypoxic and pathological conditions [10].

During the administration of general anesthesia, the entire systemic vasculature is exposed to volatile agents that exert potent modulatory effects on endothelial cell function [11]. Sevoflurane, a non-irritant volatile anesthetic and halogenated ether universally utilized for anesthesia induction and maintenance, is increasingly recognized for its capacity to alter microvascular permeability [11–14]. Because the lungs serve as the primary site of uptake and elimination for inhaled anesthetics, the pulmonary microvascular bed is exposed to the highest initial concentrations of the drug, rendering it a critical focal point for understanding anesthetic-induced vascular alterations [15,16].

Recent high-throughput transcriptomic analyses and *in vitro* functional assays indicate that sevoflurane exerts a direct, dose-dependent, and time-dependent hyperpermeability effect on both human umbilical vein endothelial cells (HUVECs) and mouse pulmonary endothelial cells (MPECs) [11,17–19]. Under sterile, baseline physiological conditions, exposure to clinically relevant concentrations of sevoflurane (equivalent to 1.5% minimum alveolar concentration) significantly increases the paracellular leakage of macromolecules, such as fluorescently labeled dextran, across the pulmonary endothelial barrier [11]. In contrast, intravenous anesthetics such as propofol fail to induce similar barrier dysfunction, indicating an agent-specific vascular response [11].

Previous studies have identified the Hypoxia-Inducible Factor 1-alpha (HIF-1α)/Vascular Endothelial Growth Factor (VEGF) axis as a downstream effector of sevoflurane-induced hyperpermeability [11]. Upon nuclear translocation, HIF-1α binds to hypoxia-response elements in target gene promoters, initiating the release of VEGF. However, HIF-1α stabilization alone under normoxic conditions fails to explain the rapid adherens junction disassembly observed, as it typically represents a delayed transcriptional event [20–22]. We hypothesize that an immediate-early transcriptional regulator rapidly responds to the biophysical stress of non-irritant volatile anesthetics, acting upstream of the HIF-1α/VEGF cascade to initiate barrier disruption.

The subsequent binding of VEGF to vascular endothelial growth factor receptor 2 (VEGFR2) triggers intracellular signaling cascades that culminate in the phosphorylation and internalization of vascular endothelial (VE)-cadherin, the core structural component of endothelial adherens junctions [23]. Concurrently, sevoflurane-induced HIF-1α activation promotes the polymerization of filamentous actin (F-actin) into robust stress fibers, generating centripetal contractile forces that physically uncouple adjacent endothelial cells. The indispensable role of this axis is evidenced by findings that targeted knockdown of HIF-1α using small interfering RNA (siRNA) completely abolishes sevoflurane-induced VEGF secretion, prevents F-actin stress fiber formation, and fully restores transendothelial electrical resistance (TEER) [11].

The physiological impact of sevoflurane on pulmonary microvascular integrity varies fundamentally depending on the pre-existing inflammatory state [24]. While it acts as a permeability enhancer in quiescent endothelium, sevoflurane demonstrates cytoprotective properties when the pulmonary endothelium is subjected to severe pre-existing inflammatory stress, such as lipopolysaccharide (LPS) exposure or ischemia-reperfusion injury [24–26]. In these contexts, sevoflurane suppresses RhoA/ROCK-mediated actomyosin contraction and mitigates endoplasmic reticulum (ER) stress by upregulating retinoid-related orphan receptor alpha (RORα), which inhibits the GRP78/p-IRE1/TRAF2 apoptotic cascade. Several studies have

demonstrated that sevoflurane reduces inflammatory cytokine release (e.g., IL-6, IL-8) and attenuates endothelial activation, protects against lung injury, and preserves endothelial glycocalyx integrity, thereby limiting vascular leakage during ischemia–reperfusion [27–29].

While the downstream effectors of anesthetic-induced vascular injury are well documented, the immediate-early transcriptional events that couple anesthetic exposure to endothelial gene regulation require further delineation. Specifically, the activation of HIF-1α by sevoflurane under normoxic conditions is mechanistically distinct from canonical hypoxia responses and does not fully explain the broad transcriptional reprogramming observed [11]. Furthermore, the aberrant localization and dysfunction of transcription factors within subcellular organelles are increasingly recognized as primary drivers of stress-induced pathological progression [30]. Endothelial barrier dysfunction is a multifactorial process, suggesting that additional immediate-early transcriptional regulators (such as EGR-1) likely function upstream of the HIF-1α/VEGF axis [31].

Although the prolonged stabilization of HIF-1α undoubtedly plays a crucial role in mediating the late-phase permeability shift observed in pulmonary microvascular endothelial cells, this does not exclude the necessary and concurrent activation of an upstream, immediate-early transcriptional response. Unlike intravenous agents, volatile anesthetics exert profound pleiotropic and physicochemical effects on cellular membranes, frequently perturbing lipid microdomains and transiently altering intracellular calcium homeostasis. These acute biophysical perturbations function as secondary messengers that initiate the rapid transcription of the Early Growth Response (EGR) family [31]. Advanced transcriptomic analyses in diverse physiological models, including the tissue-specific imprinting of pulmonary macrophages, indicate that immediate-early regulators like EGR2 serve as critical integrative hubs [32]. By linking acute physicochemical perturbations to the sustained downstream transcription of vasoactive cytokines, EGR2 orchestrates complex cellular responses. Recent *in vivo* observations reveal that sevoflurane selectively drives robust EGR2 transcription through calcium-dependent nuclear factor of activated T-cells (NFAT) signaling in neural tissues [33]. Despite this, the precise transcriptional mechanisms coupling sevoflurane exposure to endothelial gene regulation and subsequent VEGF-dependent barrier failure remain completely undefined in the pulmonary microvasculature.

Currently, whether EGR2 participates in the endothelial response to non-irritant volatile anesthetics has not been investigated. Preliminary transcriptomic sequencing of pulmonary endothelial cells exposed to sevoflurane revealed significant activation of an EGR2-VEGF transcriptional signaling axis. Given its rapid induction kinetics and regulatory role in angiogenic pathways, we hypothesize that EGR2 functions as a previously unrecognized upstream mediator linking sevoflurane exposure to VEGF-dependent endothelial barrier disruption. Elucidating the role of this EGR2-mediated pathway is essential for understanding how non-irritant volatile anesthetics initiate the transcriptional programs that destabilize pulmonary microvascular integrity.

2 Materials and Methods

2.1 Cell Culture and Sevoflurane Exposure

Human pulmonary microvascular endothelial cells (HPMECs) (ScienCell Research Laboratories, Carlsbad, CA, USA; Cat# 3000) were authenticated by Short Tandem Repeat (STR) profiling and tested negative for mycoplasma contamination. Cells were cultured in Endothelial Cell Medium (ECM; ScienCell, Cat# 1001) supplemented with 5% fetal bovine serum (FBS), 1% endothelial cell growth supplement (ECGS), and 1% penicillin/streptomycin. Cells were maintained in a humidified incubator at 37°C with 5% CO_2. For *in vitro* sevoflurane exposure, HPMECs were placed in an airtight Modular Incubator Chamber (Model

MIC-101; Billups-Rothenberg, San Diego, CA, USA). Sevoflurane (Maruishi Pharmaceutical, Osaka, Japan; Cat# 1612540) was delivered using a calibrated vaporizer (VIP 3000, Midmark, Dayton, OH, USA) with a carrier gas of 5% CO_2 and 95% room air at a flow rate of 2 L/min. The vaporizer was set to specific volume percentages, and the chamber was flushed for 15 min to allow the culture medium to equilibrate. The final dissolved concentrations in the culture medium (0.1, 0.2, and 0.3 mM) were determined based on previously established blood-gas partition coefficients and theoretical calculations at 37°C.

2.2 Trans-Endothelial (Trans-EC) Permeability Assay

HPMECs were seeded at a density of 1×10^5 cells/well onto the apical chamber of 12-well Transwell inserts (0.4 μm pore size, polycarbonate membrane; Corning Costar, Cambridge, MA, USA; Cat# 3401) and grown to post-confluence. Following treatments, 1 mg/mL of FITC-dextran (40 kDa; Sigma-Aldrich, St. Louis, MO, USA; Cat# FD40) was added to the apical chamber. After a 1-h incubation at 37°C, 100 μL aliquots were collected from the basolateral chamber. Fluorescence intensity (excitation 485 nm, emission 535 nm) was measured using a Victor X3 2030 Multimode Microplate Reader (PerkinElmer, Waltham, MA, USA). To capture the dynamic barrier alterations, measurements were taken at baseline (0 h) and subsequently at 1, 3, 6, and 12 h following exposure to a fixed concentration of 0.2 mM sevoflurane.

2.3 Transendothelial Electrical Resistance (TEER) Measurement

To assess physiological barrier integrity, TEER was measured using a Millicell ERS-2 Voltohmmeter (EMD Millipore, Billerica, MA, USA) equipped with standard chopstick electrodes. Resistance values were recorded in ohms (Ω). Background resistance from a blank insert containing only medium was subtracted, and final TEER values were calculated by multiplying by the surface area of the membrane (1.12 cm^2), expressed as $\Omega \cdot cm^2$. To capture the dynamic barrier alterations, measurements were taken at baseline (0 h) and subsequently at 1, 3, 6, and 12 h post-exposure. To avoid temperature-induced artifacts, all measurements were conducted on a heated stage maintained at 37°C within 3 min of removal from the incubator.

2.4 siRNA Transfection

To silence *EGR2* expression, HPMECs were grown to 60–70% confluence and transiently transfected with human *EGR2*-specific small interfering RNA (EGR2 siRNA) or a non-targeting negative control siRNA (NC siRNA) synthesized by GenePharma (Shanghai, China). specific sequences for human *EGR2* siRNA were 5′-GCCUUCGACCAGUGUAAUCTT-3′. Transfections were performed using Lipofectamine RNAiMAX (Thermo Fisher Scientific, Waltham, MA, USA; Cat# 13778075) at a final siRNA concentration of 50 nM according to the manufacturer's protocol. Cells were incubated for 48 h, and the knockdown efficiency was verified via Western blot analysis before downstream sevoflurane exposure.

2.5 Animal Model and In Vivo Exposure

The animal study protocol was prospectively approved by the Institutional Animal Care and Use Committee of Sichuan University (Approval No. SCU42-2512-15; Date of Approval: [10 December 2025]). All animal procedures were conducted at the Laboratory Animal Center of Sichuan University between [15 December 2025] and [15 April 2026]. The use of this facility was based on a collaboration agreement between The Third People's Hospital of Chengdu and Sichuan University. All experimental procedures were independently executed by researchers from our institution, without the participation or supervision of Sichuan University personnel. Specific pathogen-free, 6- to 8-week-old male and female C57BL/6J

mice (n = 6 per group, 3 males and 3 females) were randomly assigned to control or sevoflurane groups. Mice in the experimental group were exposed to 3.3% sevoflurane (equivalent to 1.5% minimum alveolar concentration) for 4 h in a temperature-controlled anesthetizing chamber delivered in 100% O_2 at a flow rate of 2 L/min to prevent hypoxia. Gas concentrations and physiological parameters (SpO_2, maintained > 95%, and body temperature, maintained at 37°C via a heating pad) were continuously monitored using a Datex-Ohmeda gas monitor (GE Healthcare, Chicago, IL, USA). Following exposure, animals were euthanized via cervical dislocation under deep anesthesia. Systemic blood was collected for serum isolation, and the animals were euthanized to harvest pulmonary tissues.

2.6 Histopathology and H&E Staining

Harvested mouse lungs were immediately perfused with cold PBS (1×, pH 7.4), and subsequently inflated via tracheal instillation with 4% paraformaldehyde at a constant pressure of 20 cm H_2O to prevent atelectasis. Tissues were fixed for 24 h, dehydrated through a graded ethanol series (70%, 80%, 90%, and 100%), and embedded in paraffin. Tissue blocks were sectioned at 5 μm thickness, mounted on glass slides, and stained with Hematoxylin and Eosin (H&E) (Sigma-Aldrich; #HHS16). Histopathological changes were evaluated by an independent pathologist in a blinded manner using a standardized semi-quantitative scoring system and imaged using an Olympus BX53 upright light microscope (Olympus, Tokyo, Japan).

2.7 RNA Sequencing (RNA-Seq) and Bioinformatics Analysis

Total RNA was extracted from HPMECs using TRIzol Reagent (Invitrogen, Carlsbad, CA, USA; Cat# 15596026). RNA integrity (RIN > 8.0) was verified using an Agilent 2100 Bioanalyzer (Agilent Technologies, Santa Clara, CA, USA) (n = 3 independent biological replicates per group). cDNA libraries were constructed and sequenced on an Illumina NovaSeq 6000 platform (Illumina, San Diego, CA, USA) by Novogene Co., Ltd. (Beijing, China) to generate 150 bp paired-end reads. Raw reads were quality-checked using FastQC and trimmed. Clean reads were aligned to the human reference genome (GRCh38) using STAR, and read counts were quantified using featureCounts. Differentially expressed genes (DEGs) were identified using the 'DESeq2' R package (version 1.38.0 in R software version 4.2.2) with thresholds: $|\log_2 FoldChange| > 1$ and adjusted p-value < 0.05. Gene Ontology (GO) enrichment and Protein-Protein Interaction (PPI) networks were analyzed using the STRING database (https://string-db.org/) and visualized via Cytoscape (v3.8.2).

2.8 Reverse Transcription-Quantitative PCR (RT-qPCR)

Total RNAs extracted from HPMECs and mouse lung tissues (1 μg) were reverse-transcribed into cDNA using the PrimeScript RT Reagent Kit (Takara Bio, Shiga, Japan; Cat# RR037A). RT-qPCR was performed using TB Green Premix Ex Taq II (Takara Bio; Cat# RR820A) on a QuantStudio 5 Real-Time PCR System (Applied Biosystems, Foster City, CA, USA). The thermal cycling conditions included an initial denaturation at 95°C for 30 s, followed by 40 cycles of 95°C for 5 s and 60°C for 30 s. A melt curve analysis was performed post-amplification to verify the specificity of a single product. The specific primer sequences used were: EGR2 Forward: 5′-CCTTTGACCAGATGAACGGAGTG-3′, Reverse: 5′-GAAGGTCTGGTTTCTAGGTGCAG-3′; β-actin Forward: 5′-CGCCGCCAGCTCACCATG-3′, Reverse: 5′-CACGATGGAGGGGAAGACGG-3′. Relative mRNA expression of *EGR2* was calculated using the $2^{-\Delta\Delta Ct}$) method, normalized to *β-actin*.

2.9 Western Blot Analysis

Proteins from HPMECs and homogenized mouse lung tissues were extracted using RIPA lysis buffer (Thermo Fisher Scientific; Cat# 89900) supplemented with Halt Protease and Phosphatase Inhibitor Cocktail (Thermo Fisher; Cat# 78440). Total protein concentrations were determined using a BCA Protein Assay Kit (Thermo Fisher; Cat#23225). Equal amounts of protein (30 μg) were resolved on 10% SDS-PAGE gels and transferred to 0.45 μm PVDF membranes (Millipore). Membranes were blocked with 5% non-fat milk for 1 h at room temperature and incubated overnight at 4°C with the following primary antibodies: rabbit anti-EGR2 (1:1000, Abcam, Cambridge, UK; Cat# ab43020) and mouse anti-β-actin (1:5000, Cell Signaling Technology, Danvers, MA, USA; Cat# 3700). After washing, membranes were incubated with HRP-linked anti-rabbit or anti-mouse secondary antibodies (1:3000, Cell Signaling Technology; Cat# 7074/7076) for 1 h at room temperature. Bands were visualized using SuperSignal West Pico PLUS Chemiluminescent Substrate (Thermo Fisher; Cat# 34580) and imaged on a ChemiDoc MP Imaging System (Bio-Rad, Hercules, CA, USA). The densitometric quantification of the protein bands was performed using ImageJ software (version 1.53, NIH, Bethesda, MD, USA), with protein expression levels normalized to the corresponding β-actin.

2.10 Enzyme-Linked Immunosorbent Assay (ELISA)

VEGF concentrations were quantified using the Human VEGF Quantikine ELISA Kit (R&D Systems, Minneapolis, MN, USA; Cat# DVE00) for HPMEC lysates/supernatants, and the Mouse VEGF Quantikine ELISA Kit (R&D Systems; Cat# MMV00) for mouse serum/lung lysates. Assays were conducted strictly according to the manufacturer's protocols. Absorbance was read at 450 nm with wavelength correction at 540 nm. Results for cell and tissue lysates were normalized to total protein content (pg/mg), whereas results for cell culture supernatants and mouse serum were expressed as absolute volumetric concentrations (pg/mL).

2.11 Immunofluorescence Confocal Microscopy

HPMECs cultured on glass-bottom confocal dishes were fixed with 4% paraformaldehyde for 15 min, permeabilized with 0.1% Triton X-100 for 10 min, and blocked with 5% BSA for 1 h at room temperature. Cells were incubated overnight at 4°C with primary antibodies: mouse anti-VE-cadherin (1:200, BD Pharmingen, San Diego, CA, USA; Cat# 555661) or rabbit anti-EGR2 (1:100, Abcam; Cat# ab43020). Cells were then washed and incubated for 1 h at room temperature in the dark with secondary antibodies: Alexa Fluor 488 Goat Anti-Mouse IgG (1:500, Invitrogen; Cat# A-11001) or Alexa Fluor 594 Goat Anti-Rabbit IgG (1:500, Invitrogen; Cat# A-11012). Images were acquired using a Zeiss LSM 980 confocal laser scanning microscope equipped with a 63× oil immersion objective (NA 1.40) (Carl Zeiss, Oberkochen, Germany) and analyzed using ImageJ software (Version 1.53, NIH, Bethesda, MD, USA). To quantify the structural disassembly of adherens junctions, the Mean Fluorescence Intensity (MFI) of junctional VE-cadherin was measured. The severity of junctional disruption was expressed as the percentage reduction in junctional fluorescence intensity relative to the control group, thereby ensuring that architectural analysis evaluates spatial expression density independent of cell detachment.

2.12 Statistical Analysis

All statistical analyses were performed using GraphPad Prism (version 9.0, San Diego, CA, USA). Data are presented as mean ± standard deviation (SD) from independent biological replicates. The assumption of normal distribution was formally verified using the Shapiro-Wilk test prior to applying parametric statistics.

Differences between the two groups were analyzed using an unpaired Student's *t*-test. Comparisons involving multiple groups were assessed using one-way Analysis of Variance (ANOVA) followed by Tukey's multiple comparisons test. A p-value < 0.05 was considered statistically significant.

3 Results

3.1 Sevoflurane Increases Pulmonary Microvascular Endothelial Permeability in a Dose- and Time-Dependent Manner

To evaluate the impact of sevoflurane on pulmonary microvascular barrier function, we performed transendothelial permeability assays utilizing an endothelial cell monolayer model. Our findings indicate that sevoflurane, at clinically relevant concentrations, substantially compromises the integrity of the endothelial monolayer. The permeability analysis revealed a pronounced dose-dependent response: compared to the control group (Ctr), exposure to 0.1 mM sevoflurane did not induce a significant alteration in barrier function; however, at concentrations of 0.2 mM and 0.3 mM, transendothelial permeability surged significantly, reaching approximately 2-fold ($p < 0.01$) and 2.5-fold ($p < 0.001$) of the control baseline, respectively (Fig. 1A).

Furthermore, time-course experiments at a fixed concentration (0.2 mM) uncovered a progressive deterioration of the endothelial barrier. Under sevoflurane treatment, a significant elevation in transendothelial permeability commenced at 3 h post-exposure ($p < 0.05$) and exhibited a continuous, sharp escalation with prolonged exposure. Following 6 and 12 h of exposure, permeability increased significantly ($p < 0.0001$), peaking at over 2.5 times the baseline level of the control (Fig. 1B).

To further validate the extent of barrier impairment from a biophysical perspective, we measured transendothelial electrical resistance (TEER), a highly sensitive physiological indicator of endothelial integrity. Consistent with the anomalous macromolecular tracer permeability, sevoflurane treatment precipitated a marked reduction in the TEER of the monolayer (Fig. 1C). While the control group maintained a TEER of approximately 28 Ω cm^2. The resistance in the sevoflurane-exposed group decreased to roughly 10 Ω cm^2 ($p < 0.0001$), indicating severe disruption of tight junctions and the electrophysiological barrier.

Vascular endothelial permeability is critically regulated by the physical state of endothelial adherens junctions, which are predominantly composed of VE-cadherin. To elucidate the structural basis of this functional barrier failure, we conducted high-resolution immunofluorescence imaging of VE-cadherin on the cell monolayers (Fig. 1D). In control cells, VE-cadherin exhibited a continuous, intact linear distribution at cell-cell contacts, maintaining a dense cellular network. Conversely, immunofluorescence imaging revealed that sevoflurane exposure disrupted intercellular junctions, driving a quantifiable fragmentation and lateral retraction of the VE-cadherin complex from the cell membrane. Morphological quantification corroborated these observations: the relative fluorescence intensity of junctional VE-cadherin exhibited an approximately 80% reduction in the sevoflurane group compared to the control group ($p < 0.0001$), providing a direct and quantitative reflection of severe adherens junction disassembly. Crucially, cell viability assays confirmed that this extensive junctional disruption occurs in the absence of overt cytotoxicity (Supplementary Fig. S1), demonstrating an active molecular pathway of barrier breakdown rather than cell death.

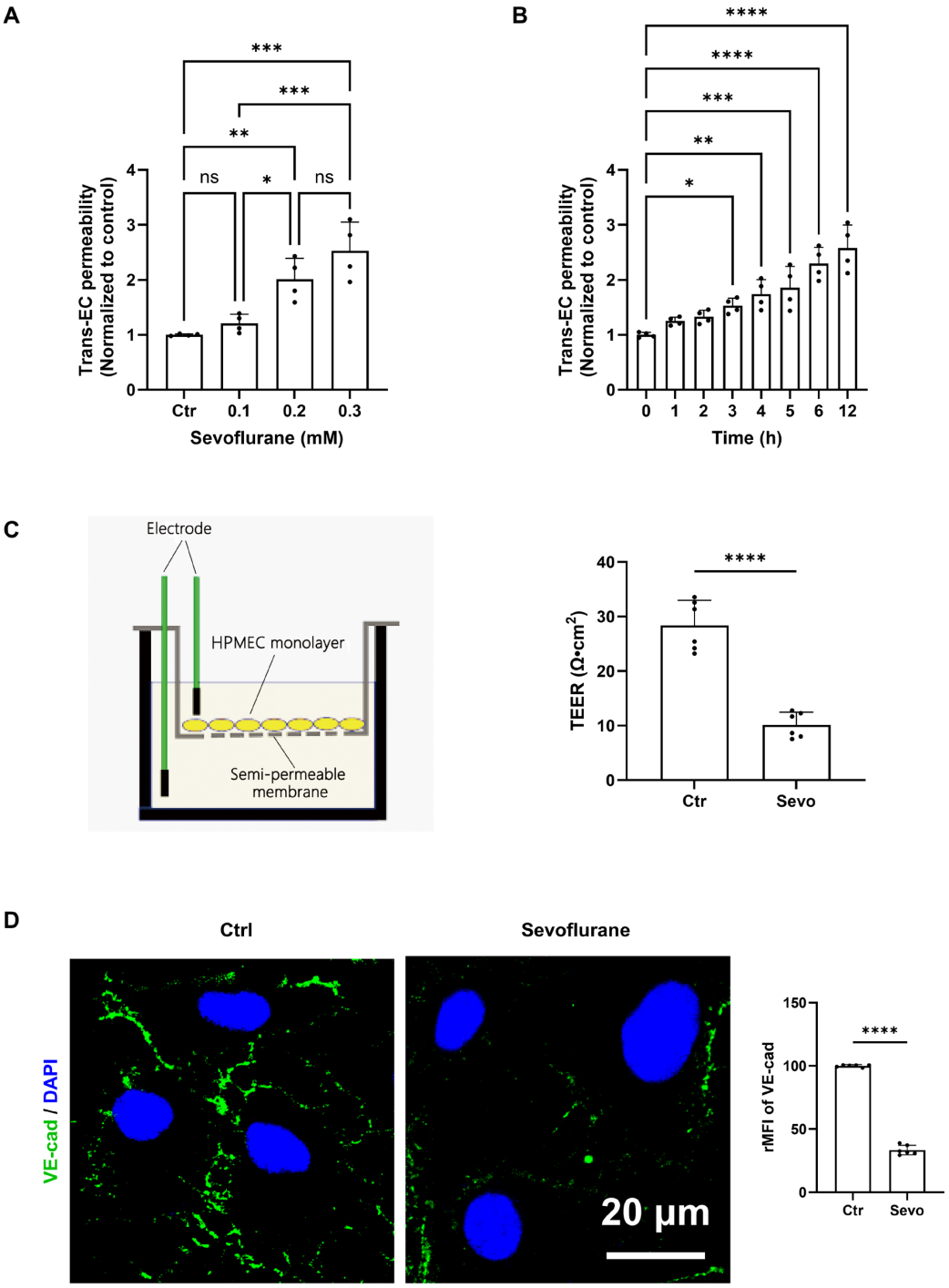

Figure 1: Sevoflurane disrupts the barrier integrity of human pulmonary microvascular endothelial cells (HPMECs) in a dose- and time-dependent manner. (**A**) Dose-dependent effect of sevoflurane on trans-endothelial (Trans-EC) permeability. HPMEC monolayers were exposed to indicated concentrations (0.1, 0.2, and 0.3 mM) of sevoflurane for 12 h. Permeability was assessed and normalized to the control (Ctr) group. (**B**) Time-course analysis of sevoflurane-induced Trans-EC permeability. HPMEC monolayers were treated with sevoflurane (0.2 mM) and evaluated at various time points ranging from 1 to 12 h. (**C**) Assessment of physiological barrier function via Transendothelial Electrical Resistance (TEER) following exposure to 0.2 mM sevoflurane for 12 h. Left: A schematic diagram illustrating the *in vitro*

TEER measurement setup using an HPMEC monolayer seeded on a semi-permeable membrane. Right: Quantification of TEER values in the control (Ctr) and sevoflurane-treated (Sevo) groups, demonstrating a significant drop in electrical resistance upon exposure. (**D**) Immunofluorescence analysis of endothelial adherens junctions following exposure to 0.2 mM sevoflurane for 12 h. Left: Representative confocal images of HPMECs stained for VE-cadherin (green) and nuclei (DAPI, blue). Scale bar: 20 μm. Sevoflurane exposure induced pronounced junctional disassembly and gap formation compared to the intact continuous network in the control. Right: Quantitative analysis of the percentage reduction in junctional VE-cadherin relative mean fluorescence intensity (rMFI). Data are presented as mean ± SD. Statistical significance was determined compared to the control group: $^{*}p < 0.05$, $^{**}p < 0.01$, $^{***}p < 0.001$, $^{****}p < 0.0001$; ns, not significant.

3.2 Transcriptomic Profiling Identifies EGR2 as a Central Hub Gene and Reveals Enhanced VEGF Expression following Sevoflurane Exposure

To elucidate the underlying molecular mechanisms driving sevoflurane-induced endothelial hyperpermeability, we performed global transcriptomic profiling using RNA sequencing (RNA-seq) on the endothelial cells exposed to 0.2 mM sevoflurane. Subsequent differential expression analysis identified a total of 295 differentially expressed genes (DEGs), comprising 174 significantly upregulated and 121 downregulated transcripts relative to the control group (threshold parameters: |log2FoldChange| > 1.0, adjusted p-value < 0.05) (Fig. 2A). Consistent with previous reports, our transcriptomic analysis also recapitulated the activation of the canonical HIF/VEGF pathway. Specifically, HIF1A and downstream VEGFA cascade transcripts exhibited significant up-regulation following sevoflurane exposure, further supporting the relevance of this axis in parallel with EGR2-driven signaling.

To identify this extensive transcriptomic shift into actionable biological pathways, a protein-protein interaction (PPI) network was constructed utilizing the highest-confidence DEGs. Topological network analysis, weighted by degree centrality, unambiguously pinpointed Early Growth Response 2 (EGR2) as the paramount central hub gene (Fig. 2B). *EGR2* exhibited dense interconnectivity with a network of notable transcription factors and signaling molecules—including ATF3, NFATC2, ID2, and NR4A1—indicating that EGR2 likely acts as a master transcriptional regulator associated with the downstream pro-angiogenic and hyperpermeability cascade initiated by non-irritant volatile anesthetic exposure.

Subsequent Gene Ontology (GO) enrichment analysis of these differentially expressed genes (DEGs) highlighted a robust enrichment in biological processes intricately linked to transcriptional regulation (e.g., negative regulation of transcription by RNA polymerase II) and cellular morphogenesis (Fig. 2C). Notably, while several enriched GO terms appear associated with disparate tissue lineages (e.g., muscle cell differentiation), this reflects the highly pleiotropic nature of immediate-early hub genes like EGR2 and ID2, which canonically govern structural remodeling and stress responses across diverse cell types, including the pulmonary endothelium.

We next sought to experimentally validate the RNA-seq findings and confirm the induction of EGR2 *in vitro*. RT-qPCR analysis demonstrated that sevoflurane treatment provoked a significant increase in *EGR2* mRNA transcription, reaching approximately 1.9-fold of the control levels ($p < 0.01$) (Fig. 2D). Corroborating this transcriptional surge, immunofluorescence staining revealed a significant accumulation of EGR2 protein. In sevoflurane-treated cells, EGR2 exhibited a highly intense, predominantly nuclear localization, with the relative mean fluorescence intensity (rMFI) surging more than 10-fold compared to baseline control levels ($p < 0.01$) (Fig. 2E).

Because vascular endothelial growth factor (VEGF) is a primary mediator of endothelial permeability and angiogenesis, we hypothesize that the prominent transcriptional alterations might culminate in

altered VEGF signaling. We quantified VEGF protein levels in both the intracellular compartment and the extracellular environment. Quantitative ELISA confirmed that sevoflurane exposure induced a robust, statistically significant elevation in both intracellular and secreted VEGF protein concentrations ($p < 0.01$) (Fig. 2F). Together, these data suggest that sevoflurane triggers a robust induction of the EGR2 regulatory network, which is closely associated with the amplified synthesis and secretion of pro-permeability factors like VEGF.

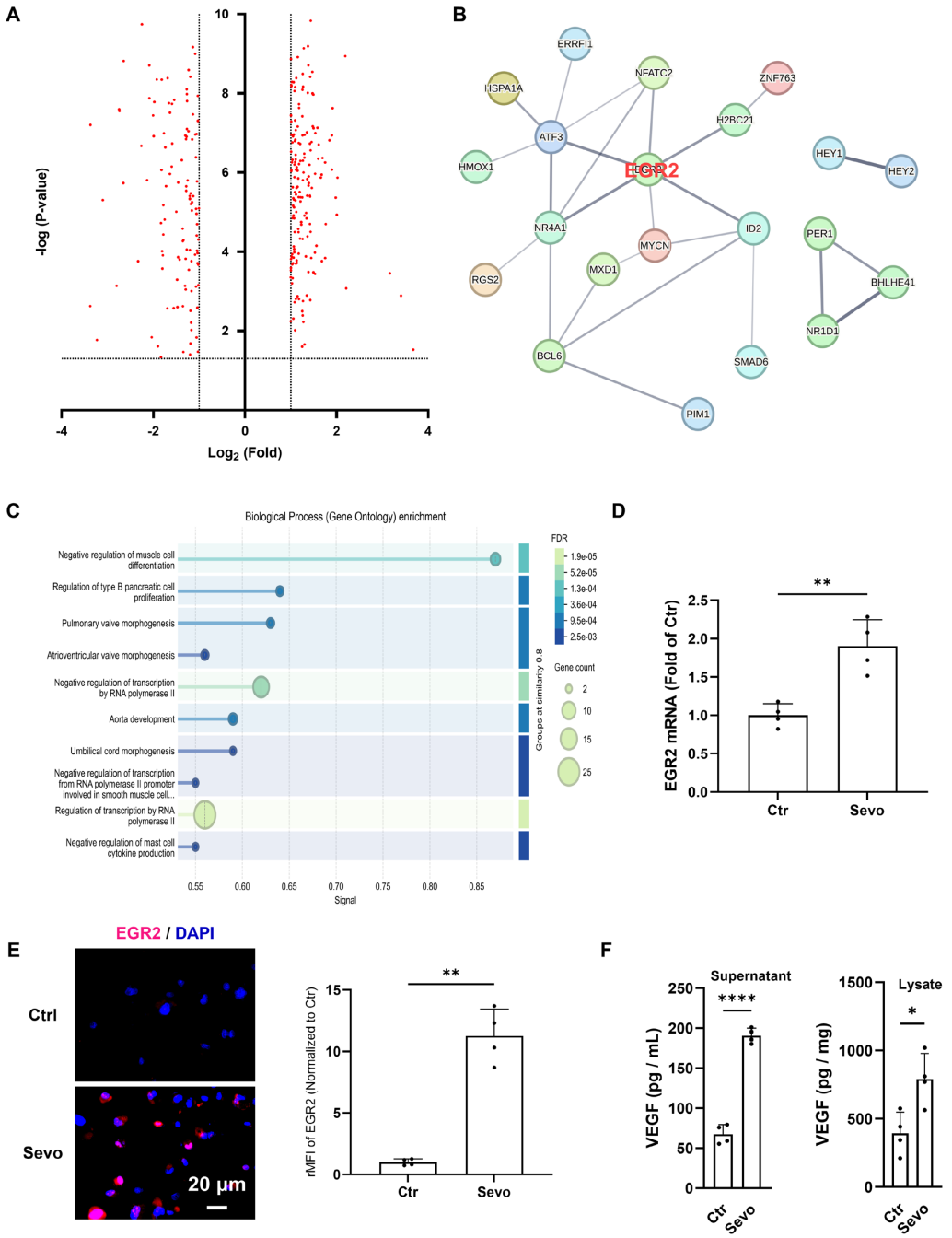

Figure 2: Transcriptomic analysis identifies upregulation of EGR2 and increased VEGF secretion in sevoflurane-treated endothelial cells. (**A**) Volcano plot of RNA-sequencing data illustrating the differentially expressed genes (DEGs)

in endothelial cells following sevoflurane exposure. Red dots denote genes with statistically significant changes in expression (thresholds indicated by the dashed lines for Log2 fold change and −Log p-value). (**B**) Interaction network map of selected DEGs. EGR2 (highlighted in red) emerges as a central hub gene, structurally linked to an array of associated transcriptional regulators and signaling molecules (e.g., ATF3, NFATC2, ID2), many of which are known to cooperate in stress-induced transcriptional reprogramming. (**C**) Gene Ontology (GO) enrichment analysis detailing the top-enriched Biological Processes among the DEGs. The size of the bubbles corresponds to the gene count within each category, the color gradient represents the False Discovery Rate (FDR), and the x-axis reflects the enrichment signal strength. (**D**) RT-qPCR validation of EGR2 mRNA expression levels in control (Ctr) and sevoflurane-treated (Sevo) groups. Data are presented as fold change relative to the control. (**E**) Immunofluorescence analysis of EGR2 protein localization and expression. Left: Representative confocal images displaying EGR2 (magenta) and nuclear counterstain (DAPI, blue). Scale bar: 20 μm. Right: Quantitative analysis of the relative mean fluorescence intensity (rMFI) of EGR2, normalized to the control group. Sevoflurane induces a marked nuclear accumulation of EGR2. (**F**) Quantification of VEGF protein concentrations in both the cell supernatant (pg/mL) and intracellular lysate (pg/mg total protein), measured via ELISA. Sevoflurane treatment significantly elevates both the synthesis and extracellular release of VEGF. Data are presented as mean ± SD. Statistical significance was determined compared to the control group: $^{*}p < 0.05$; $^{**}p < 0.01$; $^{****}p < 0.0001$.

3.3 Silencing EGR2 Abrogates Sevoflurane-Induced VEGF Upregulation and Preserves Endothelial Barrier Integrity

Having established that sevoflurane exposure robustly induces the EGR2 regulatory network and an associated surge in VEGF, we next sought to determine whether EGR2 serves as the indispensable upstream mediator of this pro-permeability cascade. To establish causality, we employed small interfering RNA (siRNA) to specifically knock down *EGR2* expression in the endothelial cells before sevoflurane exposure.

Western blot analysis confirmed the high efficacy of the targeted knockdown (Fig. 3A). In cells transfected with negative control siRNA (NC siRNA), sevoflurane provoked a significant accumulation of EGR2 protein ($p < 0.001$). Conversely, transfection with EGR2-specific siRNA effectively blunted baseline EGR2 expression and completely abolished the sevoflurane-induced protein spike. We then evaluated the downstream impact on VEGF production. In the NC siRNA group, sevoflurane triggered an extensive and highly significant elevation of VEGF in both the extracellular supernatant and intracellular lysate ($p < 0.0001$). Furthermore, the depletion of EGR2 effectively uncoupled sevoflurane exposure from VEGF synthesis; VEGF concentrations in both the supernatant and lysate of EGR2-silenced cells remained at baseline levels despite sevoflurane treatment, demonstrating no significant difference from the unexposed controls (Fig. 3B).

To definitively link this molecular mechanism to the physiological barrier phenotype, we assessed the functional endpoints of transendothelial permeability and electrical resistance in the context of EGR2 depletion. As expected, sevoflurane elicited a significant decrease in Transendothelial Electrical Resistance (TEER) ($p < 0.0001$) (Fig. 3C) and a concomitant surge in macromolecular permeability ($p < 0.0001$) (Fig. 3D) in the NC siRNA control group. However, targeted silencing of EGR2 imparted a near-complete restoration of barrier function. In EGR2-depleted monolayers, sevoflurane failed to induce a significant reduction in TEER (Fig. 3C). Furthermore, the sevoflurane-driven hyperpermeability was entirely mitigated; in fact, trans-EC permeability in the EGR2 siRNA + sevoflurane group exhibited a slight, statistically significant reduction below baseline levels ($p < 0.05$) compared to its respective control (Fig. 3D). This minor barrier-tightening effect likely reflects the ablation of basal EGR2/VEGF signaling pathways that maintain native junctional turnover. Taken together, these data provide compelling evidence that EGR2 is mechanically

indispensable for sevoflurane-induced endothelial barrier dysfunction, acting as a critical transcriptional node that drives the pathogenic VEGF response.

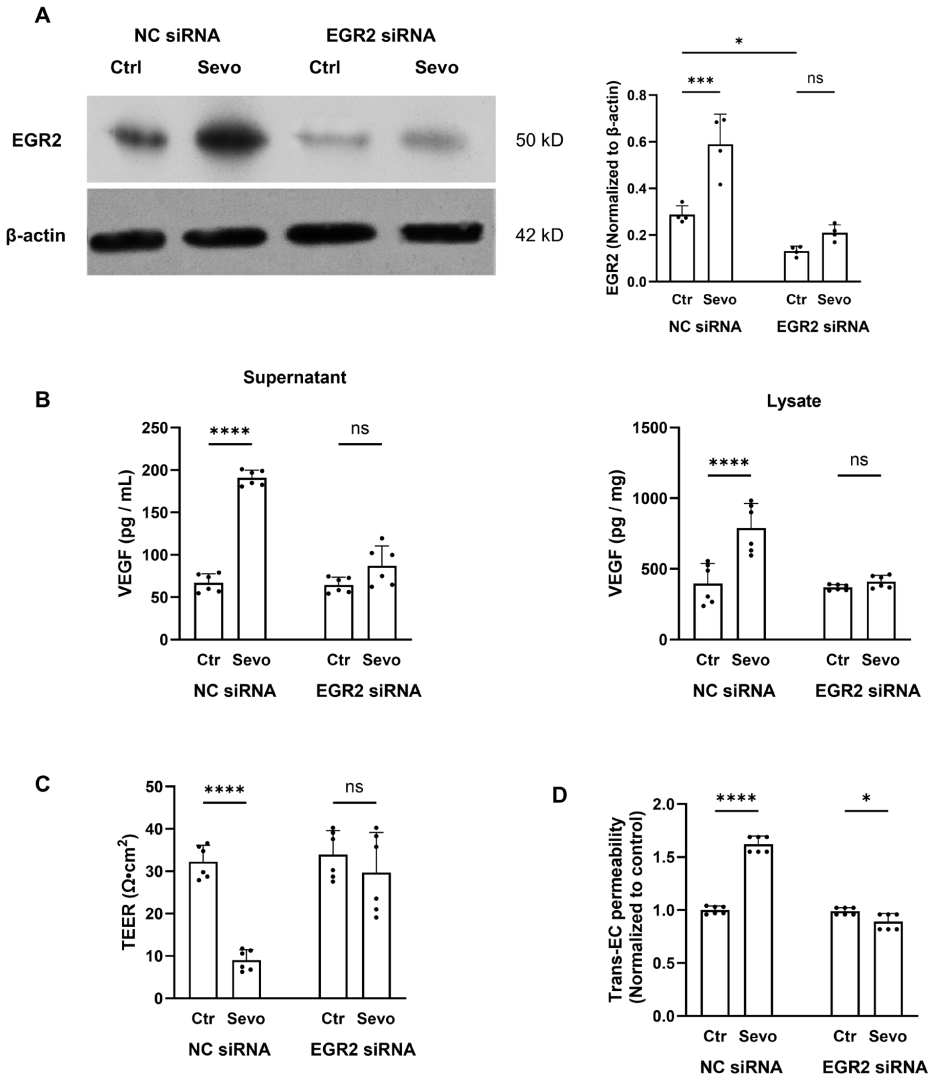

Figure 3: EGR2 silencing completely prevents sevoflurane-induced VEGF overproduction and endothelial barrier disruption. (**A**) Western blot analysis of EGR2 protein levels following transfection with negative control siRNA (NC siRNA) or EGR2-targeted siRNA (EGR2 siRNA), with or without sevoflurane (Sevo) exposure. *Left*: Representative immunoblots for EGR2 (50 kD) and the loading control β-actin (42 kD). *Right*: Densitometric quantification of EGR2 normalized to β-actin. EGR2 siRNA successfully ablates the sevoflurane-induced protein spike. (**B**) Quantification of VEGF protein concentrations via ELISA. Left: Secreted VEGF in the cell supernatant (pg/mL and intracellular VEGF in the lysate normalized to total protein (pg/mg). Silencing EGR2 eliminates the sevoflurane-driven surge in VEGF production and secretion. (**C**) Assessment of physiological barrier integrity using Transendothelial Electrical Resistance (TEER). EGR2 knockdown prevents the drastic, sevoflurane-induced loss of electrical resistance observed in the NC siRNA group. (**D**) Functional assay of trans-endothelial (Trans-EC) permeability. Data are normalized to the NC siRNA control. Depletion of EGR2 restores the monolayer from sevoflurane-induced hyperpermeability. Data are presented as mean ± SD. Statistical significance was determined between the indicated groups: $^{*}p < 0.05$, $^{***}p < 0.001$, $^{****}p < 0.0001$; ns, not significant.

3.4 Sevoflurane Induces Pulmonary Vascular Injury and Activates the EGR2/VEGF Axis In Vivo

To determine whether the sevoflurane-driven transcriptional reprogramming and subsequent endothelial barrier dysfunction observed *in vitro* translate to an *in vivo* physiological system, we utilized a murine model of general anesthesia exposure.

We first performed a histopathological evaluation of the pulmonary architecture using Hematoxylin and Eosin (H&E) staining (Fig. 4A). Lung sections from the control group displayed normal, delicate alveolar septa and clear alveolar spaces. In stark contrast, lung tissues from sevoflurane-treated mice exhibited pronounced morphological deterioration. The sevoflurane group showed widespread vascular congestion, marked thickening of the alveolar walls, and the presence of proteinaceous exudate within the alveolar spaces. These pathological features strongly indicate acute pulmonary microvascular leakage and an overall breakdown of the *in vivo* lung endothelial barrier.

To confirm that the EGR2/VEGF signaling axis is responsible for mediating this *in vivo* vascular injury, we harvested lung tissues and systemic blood from the animals. Corroborating our transcriptomic data, quantitative real-time PCR (RT-qPCR) revealed that sevoflurane exposure provoked a significant upregulation of *EGR2* mRNA in the whole lung tissue, reaching approximately 1.5-fold of the baseline control ($p < 0.01$) (Fig. 4B). This transcriptional induction was faithfully mirrored at the protein level. Western blot analysis of the lung lysates demonstrated a robust and highly significant accumulation of EGR2 protein in the sevoflurane-exposed cohort compared to the vehicle controls ($p < 0.001$) (Fig. 4C).

Finally, we assessed the downstream functional output of this regulatory cascade by quantifying VEGF levels. ELISA analysis demonstrated that sevoflurane exposure not only significantly increased VEGF concentrations locally within the pulmonary microenvironment (lung lysate, $p < 0.05$) but also triggered a substantial elevation of VEGF in the systemic circulation (serum, $p < 0.01$) (Fig. 4D). Taken together, these *in vivo* findings reinforce our *in vitro* mechanistic framework, implicating the pulmonary and systemic EGR2/VEGF signaling axis as a key mediator of sevoflurane-induced impairment of pulmonary vascular integrity.

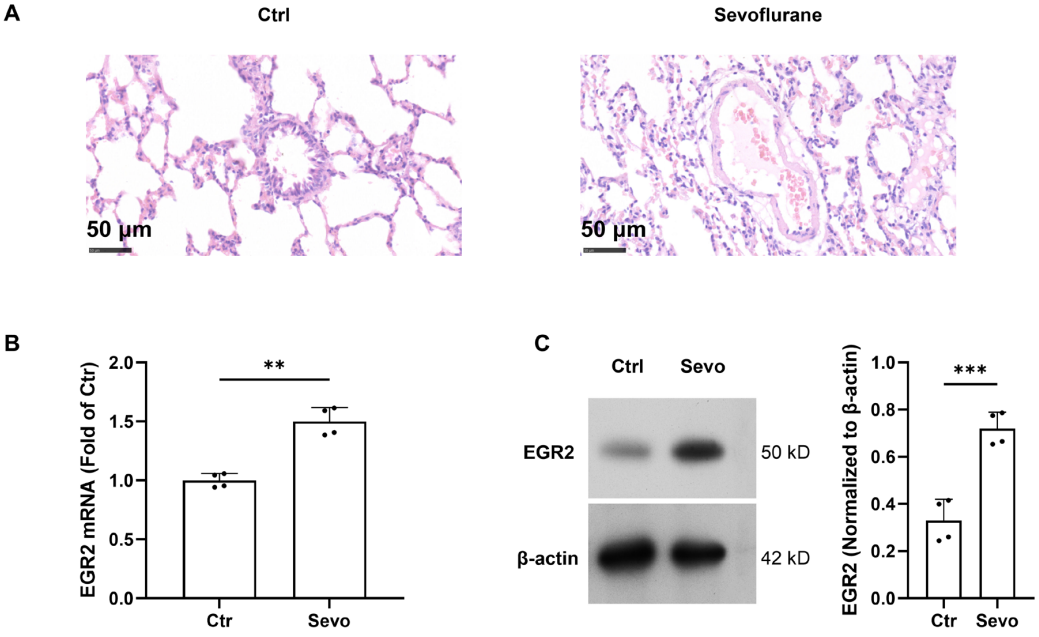

Figure 4: *Cont.*

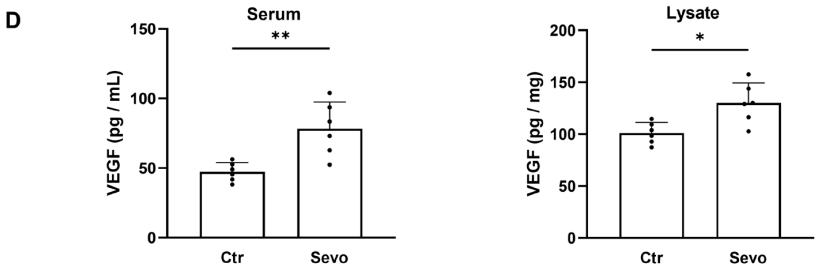

Figure 4: Sevoflurane compromises pulmonary vascular integrity and upregulates the EGR2/VEGF axis *in vivo*. (**A**) Representative Hematoxylin and Eosin (H&E) stained images of lung sections from control (Ctrl) and sevoflurane-treated (Sevo) mice. Sevoflurane exposure induces severe histopathological alterations, including marked vascular congestion, interstitial thickening, and alveolar exudate, indicative of increased pulmonary vascular permeability. Scale bars = 50 μm. (**B**) RT-qPCR analysis of *EGR2* mRNA expression in murine lung tissues following sevoflurane exposure. Data are expressed as fold change relative to the Ctrl group. (**C**) Western blot analysis (*left*) and corresponding densitometric quantification (*right*) of EGR2 protein expression in lung lysates. β-actin was used as the internal loading control. Sevoflurane triggers a highly significant accumulation of EGR2 protein *in vivo*. (**D**) Quantification of VEGF protein concentrations in the systemic circulation (Serum, pg/mL) and local pulmonary tissue (Lysate, pg/mg, normalized to total protein) via ELISA. Sevoflurane exposure leads to a significant increase in both systemic and localized VEGF production. Data are presented as mean ± SD. Statistical significance was determined compared to the control group: $^{*}p < 0.05$, $^{**}p < 0.01$, $^{***}p < 0.001$.

4 Discussion

The pulmonary microvascular endothelium is essential for gas exchange and fluid homeostasis [11,34]. Although sevoflurane is widely used in general anesthesia, its specific impact on endothelial function remains unclear, and it may influence outcomes in susceptible surgical patients. In this study, we systematically delineate a genetically encoded pathway through which sevoflurane provokes pulmonary microvascular barrier dysfunction. By combining *in vitro* monolayer models with *in vivo* physiological assessments, we demonstrate that clinically relevant exposures to sevoflurane trigger a transcriptional reprogramming event, culminating in the aberrant activation of the Early Growth Response 2 (EGR2)/Vascular Endothelial Growth Factor (VEGF) signaling axis. These findings provide a vital molecular framework for understanding the iatrogenic vulnerabilities of the pulmonary microvasculature during general anesthesia.

We establish a precise, dose- and time-dependent threshold for sevoflurane-induced endothelial barrier failure. Exposure to concentrations mimicking deep surgical anesthesia (0.2 mM, approximately equivalent to 1.5% minimum alveolar concentration) rapidly precipitates a severe deterioration of transendothelial electrical resistance (TEER) alongside a concomitant surge in macromolecular permeability. This observation aligns with recent independent investigations demonstrating that sevoflurane, at clinically relevant concentrations, disrupts the endothelial monolayer formed by various human and murine endothelial cells in transwell permeability models [11,25]. Importantly, our temporal kinetic data reveal that brief exposures are well-tolerated, whereas continuous exposure exceeding three hours initiates an exponential decline in barrier integrity. The structural basis for this functional collapse is the extensive disassembly and retraction of VE-cadherin at the adherens junctions [35]. Unlike the transient, highly regulated gap formations characteristic of physiological angiogenesis or acute leukocyte extravasation, prolonged sevoflurane exposure induces a sustained, pathological fragmentation of the VE-cadherin network. This transforms the highly restrictive pulmonary endothelium into a leaky, pro-exudative phenotype, providing a direct

cellular rationale for the increased risk of postoperative pulmonary edema frequently observed following prolonged surgical procedures under non-irritant volatile anesthesia [6].

The major finding of the present study lies in the identification of EGR2 as the central transcriptional hub orchestrating this anesthetic-induced barrier dysfunction. To date, the molecular mechanisms linking non-irritant volatile anesthetics to endothelial hyperpermeability have remained incompletely explored. While recent seminal studies have elegantly demonstrated that sevoflurane induces the expression and activation of hypoxia-inducible factor 1α (HIF-1α), which subsequently mediates endothelial permeability, our unbiased, genome-wide transcriptomic profiling demonstrates EGR2 as an equally critical and perhaps parallel master regulator. While EGR2 is traditionally recognized for its developmental roles in peripheral nerve myelination and immune tolerance [36–39], our data uniquely position it as a robust, stress-responsive transcription factor within the pulmonary microvasculature [33]. We found that sevoflurane exposure triggers the rapid upregulation and extensive nuclear accumulation of EGR2. Importantly, targeted loss-of-function experiments using siRNA completely abrogated the sevoflurane-induced functional decline, fully restoring physiological TEER and mitigating macromolecular hyperpermeability. This definitive functional rescue establishes EGR2 not merely as a correlative downstream biomarker of anesthetic stress, but as an indispensable molecular executor of barrier disruption.

EGR2/VEGF axis as a center event of anesthetic-induced barrier dysfunction provides a compelling mechanistic foundation for the disparate vascular profiles observed between diverse clinical anesthetic regimens [40]. Recent rigorous comparative investigations have elucidated that clinically relevant exposures to sevoflurane inherently drive HIF-1α stabilization and ensuing VEGF elaboration in pulmonary endothelial tissues, thereby precipitating significant microvascular leakage, whereas intravenous agents such as propofol exert no such detrimental influence under normoxic baseline conditions [11]. Our findings significantly advance this paradigm by identifying EGR2 as the principal, immediate-early transcriptional sensor uniquely sensitive to non-irritant volatile anesthetic exposure. We hypothesize that the distinct physicochemical properties of halogenated ethers, which partition into endothelial cell membranes and alter lipid raft microdomains, may trigger secondary messenger cascades such as cytosolic calcium transients. These immediate biophysical perturbations likely serve as the upstream cue for the rapid calcineurin/NFAT-mediated EGR2 transactivation, an intracellular signaling cascade entirely bypassed by non-lipid-perturbing agents like propofol. However, we acknowledge that this upstream cascade remains a speculative hypothesis in our current study. Future research incorporating calcium chelators, calcineurin inhibitors, or comparative parallel treatments is required to functionally validate whether this specific pathway is indeed uniquely triggered by non-irritant volatile agents. Consequently, in complex perioperative scenarios characterized by a pre-existing vulnerability of the endothelial glycocalyx and intercellular junctions—such as during massive fluid resuscitation, severe sepsis, or extensive oncological resections—the inherent pro-permeability attributes of sevoflurane, mediated via this newly characterized EGR2 network, could act as a potent deleterious ‘second hit’. This synergistic exacerbation of endothelial gap formation provides a vital molecular rationale for critically evaluating anesthetic selection. While these findings are still at an early, exploratory stage, they suggest that further investigation into targeting the EGR2/VEGF axis might inform future perioperative strategies. However, given the variability in patient populations, inflammatory states, and clinical contexts, such translational implications require substantially stronger validation.

Downstream of this transcriptional activation, we identified VEGF as the primary pathogenic effector bridging EGR2 upregulation to physical junctional failure. Sevoflurane exposure drove an increased secretion of VEGF, a phenomenon that was entirely extinguished upon EGR2 silencing. VEGF is classically established as one of the most potent regulators of endothelial function, known to increase vascular

permeability by promoting the reorganization of endothelial cell junctions such as zonula occludens-1 and occludin [1,41–43]. Furthermore, our *in vitro* findings are consistent with emerging clinical observations in which the perioperative studies have reported that surgical cancer patients receiving sevoflurane anesthesia exhibit significantly higher systemic levels of VEGF compared to those receiving intravenous anesthetics like propofol [44]. By positioning EGR2 directly upstream of this VEGF surge, our study bridges the gap between anesthetic-induced transcriptional stress and the clinically observed pro-angiogenic, pro-permeability phenotypes.

Consistent with these *in vitro* mechanisms, our murine models demonstrated activation of the EGR2/VEGF signaling axis. Inhalational exposure to sevoflurane faithfully mirrored the *in vitro* transcriptional signature, provoking significant EGR2 accumulation and VEGF overproduction within both the local pulmonary microenvironment and the systemic circulation [11]. This molecular dysregulation manifested histologically as acute pulmonary vascular congestion, interstitial thickening, and alveolar proteinaceous exudate [34]. Notably, the induction of pulmonary vascular leakage by sevoflurane has been corroborated by *in vivo* imaging studies utilizing fluorescent tracers such as AngioSense 750 and rhodamine-labeled dextran, which demonstrate substantial dye accumulation in the lung parenchyma following sevoflurane exposure [11]. It is highly pertinent to contrast these detrimental effects of sevoflurane with the profile of intravenous anesthetics. Existing literature indicates that propofol does not significantly perturb endothelial permeability or induce HIF-1α/VEGF activation at clinical doses [11,29]. This stark divergence highlights a specific pharmacological liability of non-irritant volatile anesthetics, suggesting that the entire vasculature of the body, when exposed to inhaled sevoflurane, undergoes unique membrane and physicochemical perturbations that activate the EGR2 network.

Despite these findings, several limitations warrant consideration. First, the *in vitro* HPMEC transwell model lacks the physiological fluid shear stress exerted by pulmonary blood flow, a critical biomechanical factor that natively modulates endothelial junctional integrity. Second, while EGR2 is robustly upregulated, the exact initial sensor—such as specific mechanosensitive ion channels (e.g., Piezo1 or TRPV4) or altered membrane lipid dynamics—responsible for detecting sevoflurane's insertion remains uncharacterized [45–47]. Future research incorporating microfluidic dynamic culture systems and electrophysiological evaluations is necessary to fully delineate this membrane-to-nucleus signaling axis.

5 Conclusion

In conclusion, our findings elucidate a previously unrecognized, genetically encoded cascade through which sevoflurane compromises pulmonary microvascular integrity in preclinical models [32]. By pinpointing the EGR2/VEGF axis as a key mediator of anesthetic-induced endothelial hyperpermeability, this study provides a mechanistic foundation for further exploratory research. The clinical implications of this anesthetic-induced baseline hyperpermeability are substantial, particularly for highly vulnerable surgical populations—such as those undergoing major trauma, tumor resections, or suffering from sepsis—where the endothelium is already primed by systemic inflammation. In such scenarios, sevoflurane may act as a deleterious "second hit," synergizing with circulating cytokines to precipitate acute respiratory distress syndrome or severe systemic edema. Future research should focus on elucidating the upstream mechanisms driving EGR2 induction following sevoflurane exposure, including the potential interplay with alveolar and bronchial epithelial cells.

Acknowledgement: None.

Funding Statement: This study was funded by the Special Research Fund for Perioperative Comprehensive Management of Obese Patients, Chengdu Hi-Tech Medical Association (Grant No. 2025001).

Author Contributions: The authors confirm contribution to the paper as follows: Conceptualization, Zhuyuan Ren and Qiang Fu; methodology, Zhuyuan Ren, Qiang Li and Qiang Fu; validation, Zhuyuan Ren, Qiang Li and Qiang Fu; investigation, Zhuyuan Ren, Yong Chen, JiaqiaoWu, Qiang Li and Qiang Fu; writing—original draft preparation, Zhuyuan Ren and Qiang Fu; writing—review and editing, Zhuyuan Ren, Qiang Li and Qiang Fu; visualization, Zhuyuan Ren, Yong Chen, Jiaqiao Wu, Qiang Li and Qiang Fu. All authors reviewed and approved the final version of the manuscript.

Availability of Data and Materials: The authors confirm that the data supporting the findings of this study are available within the article.

Ethics Approval: All animal procedures were approved prior to the commencement of the study by the Institutional Animal Care and Use Committee (IACUC) of Sichuan University (Approval No. SCU42-2512-15, Date of Approval: [10 December 2025]) and adhered to the Guide for the Care and Use of Laboratory Animals. The animal experiments were conducted at the Laboratory Animal Center of Sichuan University under an institutional agreement. Under this framework, our research team was granted official access to utilize the facility and receive basic animal husbandry services. We explicitly confirm that all experimental procedures, data collection, and subsequent analyses were independently performed by our team members from The Third People's Hospital of Chengdu. Personnel from Sichuan University did not participate in, supervise, or provide guidance for the experimental design or execution.

Conflicts of Interest: The authors declare no conflicts of interest.

Supplementary Materials: The supplementary material is available online at https://www.techscience.com/doi/10.32604/biocell.2026.085300/s1.

References

1. Zeng Y, Fu BM. Angiogenesis and microvascular permeability. Cold Spring Harb Perspect Med. 2025;15(1):a041163. [CrossRef].
2. Qiu Y, Chang S, Zeng Y, Wang X. Advances in mitochondrial dysfunction and its role in cardiovascular diseases. Cells. 2025;14(20):1621. [CrossRef].
3. Jin L, Qin Y, Zhao Y, Zhou X, Zeng Y. Endothelial cytoskeleton in mechanotransduction and vascular diseases. J Biomech. 2025;182:112579. [CrossRef].
4. Liu M, Li X, Liu J, Liu Y. Tanshinone IIA inhibits NLRP3 activation and attenuates alveolar macrophage pyroptosis via the TREM2/β-catenin pathway. Biocell. 2024;48(10):1475–87. [CrossRef].
5. He X, Jin L, Qin Y, Zhong J, Ouyang Z, Zeng Y. Advances in micropillar arrays in cellular biomechanics detection and tissue engineering. Biocell. 2024;48(11):1521–9. [CrossRef].
6. Weis SM, Cheresh DA. Pathophysiological consequences of VEGF-induced vascular permeability. Nature. 2005;437(7058):497–504. [CrossRef].
7. Gkaifyllia A, Bruzek S, Ignjatovic V, Pober JS, Sochet AA, Pierce RW. Distinct blood and lung proteins drive pulmonary capillary leak in children with severe hypoxemic respiratory failure. Pediatr Crit Care Med. 2026;27(5):634–45. [CrossRef].
8. Omasa K, Suzuki Y. Viscous sputum and systemic edema: Key physical signs for transfusion-related acute lung injury diagnosis during anesthesia. Cureus. 2025;17(12):e99430. [CrossRef].
9. Rong YY, Li YW, Yang SY, Liu SY, Dong YH, Du HB, et al. The role of TIPE2 in hemorrhagic shock-induced acute lung injury. Acta Cir Bras. 2026;41:e410326. [CrossRef].
10. Gornostaeva A, Buravkova L, Lobanova M, Andreeva E. HIFs in hypoxic regulation of the extracellular matrix: Focus on little-known player HIF-3. Biocell. 2024;48(5):677–92. [CrossRef].

11. Li R, Huang Y, Lin K, Li X, Dilger JP, Lin J. Distinct effects of sevoflurane and propofol on vascular permeability *in vitro* and in a mouse model. Anesthesiology. 2025;142(6):1058–70. [CrossRef].
12. Ahn Y, Patil CD, Nozohouri E, Zoubi S, Patel D, Bickel U. Higher brain uptake of gentamicin and ceftazidime under isoflurane anesthesia compared to ketamine/xylazine. Pharmaceutics. 2024;16(1):135. [CrossRef].
13. Noorani B, Chowdhury EA, Alqahtani F, Ahn Y, Nozohouri E, Zoubi S, et al. Effects of volatile anesthetics versus ketamine on blood-brain barrier permeability via lipid-mediated alterations of endothelial cell membranes. J Pharmacol Exp Ther. 2023;385(2):135–45. [CrossRef].
14. Xue Y, Jia L, Zhang J, Ni S. Sevoflurane postconditioning regulates mitophagy through the PINK1/parkin pathway to alleviate myocardial microcirculatory reperfusion injury. Chem Biol Drug Des. 2025;106(6):e70228. [CrossRef].
15. Riess ML, Novalija E, Camara AKS, Eells JT, Chen Q, Stowe DF. Preconditioning with sevoflurane reduces changes in nicotinamide adenine dinucleotide during ischemia-reperfusion in isolated hearts: Reversal by 5-hydroxydecanoic acid. Anesthesiology. 2003;98(2):387–95. [CrossRef].
16. Fukuda S, Niimi Y, Sekiya Y, Manyeza E, Jacob S, Cox RA, et al. Selective hemoadsorption of cytokines and platelet-neutrophil complexes mitigates lung microvascular hyperpermeability in an ovine acute lung injury model. Intensive Care Med Exp. 2026;14(1):41. [CrossRef].
17. Lu W, Ai Q, Wang Z, Zhang T, Deng S, He J, et al. Perioperative inflammation, anesthesia modulation and cellular signaling in lung cancer: An integrated transcriptomic and single-cell analysis. Transl Lung Cancer Res. 2026;15(4):78. [CrossRef].
18. Urner M, Schläpfer M, Herrmann IK, Hasler M, Schimmer RR, Booy C, et al. Insight into the beneficial immunomodulatory mechanism of the sevoflurane metabolite hexafluoro-2-propanol in a rat model of endotoxaemia. Clin Exp Immunol. 2015;181(3):468–79. [CrossRef].
19. Zhang L, Xu L. Fgf2 and Ptpn11 play a role in cerebral injury caused by sevoflurane anesthesia. Medicine. 2023;102(45):e36108. [CrossRef].
20. Liang Y, Su T, Zhu S, Sun R, Qin J, Yue Z, et al. *Astragali radix-Curcumae rhizoma* normalizes tumor blood vessels by HIF-1α to anti-tumor metastasis in colon cancer. Phytomedicine. 2025;140:156562. [CrossRef].
21. Lin L, Bi H, Yang J, Shang Y, Lv Q, Zhang D, et al. *Pasteurella multocida* infection induces blood-brain barrier disruption by decreasing tight junctions and adherens junctions between neighbored brain microvascular endothelial cells. Vet Res. 2024;55(1):104. [CrossRef].
22. Springer M, Burakgazi ZA, Domukhovska A, Nafchi B, Beary MC, Acquisto A, et al. HIF-1α-mediated disruption of cellular junctions: The impact of hypoxia on the tumor microenvironment and invasion. Int J Mol Sci. 2025;26(11):5101. [CrossRef].
23. Gavard J, Gutkind JS. VEGF controls endothelial-cell permeability by promoting the beta-arrestin-dependent endocytosis of VE-cadherin. Nat Cell Biol. 2006;8(11):1223–34. [CrossRef].
24. Ni W, Zou Z, Jiang P, Wang S. Sevoflurane alleviates inflammation, apoptosis and permeability damage of human umbilical vein endothelial cells induced by lipopolysaccharide by inhibiting endoplasmic reticulum stress via upregulating RORα. Prostaglandins Other Lipid Mediat. 2024;172:106821. [CrossRef].
25. Huang Y, Tan Q, Chen R, Cao B, Li W. Sevoflurane prevents lipopolysaccharide-induced barrier dysfunction in human lung microvascular endothelial cells: Rho-mediated alterations of VE-cadherin. Biochem Biophys Res Commun. 2015;468(1–2):119–24. [CrossRef].
26. Restin T, Kajdi ME, Schläpfer M, Roth Z'graggen B, Booy C, Dumrese C, et al. Sevoflurane protects rat brain endothelial barrier structure and function after hypoxia-reoxygenation injury. PLoS One. 2017;12(10):e0184973. [CrossRef].
27. O'Gara B, Talmor D. Lung protective properties of the volatile anesthetics. Intensive Care Med. 2016;42(9):1487–9. [CrossRef].
28. Zhai R, Lenga Ma Bonda W, Leclaire C, Saint-Béat C, Theilliere C, Belville C, et al. Effects of sevoflurane on lung epithelial permeability in experimental models of acute respiratory distress syndrome. J Transl Med. 2023;21(1):397. [CrossRef].
29. Kim HJ, Kim E, Baek SH, Kim HY, Kim JY, Park J, et al. Sevoflurane did not show better protective effect on endothelial glycocalyx layer compared to propofol during lung resection surgery with one lung ventilation. J Thorac Dis. 2018;10(3):1468–75. [CrossRef].

30. Zeng Y, Fu BM. Subcellular organelles and cellular molecules: Localization, detection, prediction, and diseases. Biocell. 2025;49(6):925–30. [CrossRef].
31. Thiel G, Cibelli G. Regulation of life and death by the zinc finger transcription factor Egr-1. J Cell Physiol. 2002;193(3):287–92. [CrossRef].
32. McCowan J, Fercoq F, Kirkwood PM, T'Jonck W, Hegarty LM, Mawer CM, et al. The transcription factor EGR2 is indispensable for tissue-specific imprinting of alveolar macrophages in health and tissue repair. Sci Immunol. 2021;6(65):eabj2132. [CrossRef].
33. Chen YR, Zhang SX, Fang M, Zhang P, Zhou YF, Yu X, et al. Egr2 contributes to age-dependent vulnerability to sevoflurane-induced cognitive deficits in mice. Acta Pharmacol Sin. 2022;43(11):2828–40. [CrossRef].
34. Su Y, Lucas R, Fulton DJR, Verin AD. Mechanisms of pulmonary endothelial barrier dysfunction in acute lung injury and acute respiratory distress syndrome. Chin Med J Pulm Crit Care Med. 2024;2(2):80–7. [CrossRef].
35. Parinandi N, Gerasimovskaya E, Verin A. Editorial: Molecular mechanisms of lung endothelial permeability. Front Physiol. 2022;13:976873. [CrossRef].
36. Bang JY, Lim NK. Synergistic enhancement of peripheral nerve regeneration via ibudilast-primed three-dimensional spheroid culture of human adipose-derived stem cells. Pharmaceuticals. 2026;19(2):335. [CrossRef].
37. Chrysostomaki M, Chatzi D, Kyriakoudi SA, Meditskou S, Manthou ME, Gargani S, et al. Hereditary polyneuropathies in the era of precision medicine: Genetic complexity and emerging strategies. Genes. 2026;17(1):56. [CrossRef].
38. Masle-Farquhar E, Peters TJ, Miosge LA, Parish IA, Weigel C, Oakes CC, et al. Uncontrolled CD21low age-associated and B1 B cell accumulation caused by failure of an EGR2/3 tolerance checkpoint. Cell Rep. 2022;38(3):110259. [CrossRef].
39. Wagle MV, Vervoort SJ, Kelly MJ, Van Der Byl W, Peters TJ, Martin BP, et al. Antigen-driven EGR2 expression is required for exhausted $CD8^+$ T cell stability and maintenance. Nat Commun. 2021;12:2782. [CrossRef].
40. Kolostyak Z, Bojcsuk D, Baksa V, Szigeti ZM, Bene K, Czimmerer Z, et al. EGR2 is an epigenomic regulator of phagocytosis and antifungal immunity in alveolar macrophages. JCI Insight. 2024;9(17):e164009. [CrossRef].
41. Lee C, Kim MJ, Kumar A, Lee HW, Yang Y, Kim Y. Vascular endothelial growth factor signaling in health and disease: From molecular mechanisms to therapeutic perspectives. Signal Transduct Target Ther. 2025;10:170. [CrossRef].
42. Wang N, Yao F, Xu W, Feng T, Li Z, Zhang Q, et al. The transcription factor islet-1 regulates diabetes-induced inner blood-retinal barrier disruption. Investig Ophthalmol Vis Sci. 2025;66(13):8. [CrossRef].
43. Li Y, Zhou F, You J, Gong X. Annexin A1 mitigates blood–brain barrier disruption in a sepsis-associated encephalopathy model by enhancing the expression of occludin and zonula occludens-1 (ZO-1). CNS Neurosci Ther. 2024;30(12):e70173. [CrossRef].
44. Yang S, Hu X, Han Y. Effect of thoracic paraspinal block-propofol intravenous general anesthesia on VEGF and TGF-β in patients receiving radical resection of lung cancer. Medicine. 2019;98(47):e18088. [CrossRef].
45. Qiu X, Liu H, Yao S, Zheng F, Yao P, Zhao H. Piezo1: A potential therapeutic target for endothelial dysfunction-related diseases. Life Sci. 2026;397:124424. [CrossRef].
46. Teixeira SPB, Pardo A, Taboada P, Bijonowski BM, Carvalho MT, Nieder JB, et al. Submolecular modulation of PIEZO1 mechanotransduction with wireless tailor-made nanoswitches. Bioact Mater. 2026;63:904–23. [CrossRef].
47. Pabst A, Brock N, Hardt S, Grannemann CCF, Kubiza H, Thiebes AL, et al. Mechanoresponsive ion channels Piezo1 and TRPV4 stimulate ADAM10 and ADAM17 with differential impact on endothelial migration and proliferation. Cell Commun Signal. 2026;24(1):52. [CrossRef].